Supporting Information

Coordinated Assembly of A novel 3D Mesoporous Fe_3O_4@Cu_2O-Graphene Oxide Framework As Highly Efficient and Reusable Catalysts for the Synthesis of Quinoxalines

Zhiyi Wang, Guowen Hu, Jian Liu, Weisheng Liu, Haoli Zhang, and Baodui Wang*

Key Laboratory of Nonferrous Metal Chemistry and Resources Utilization of Gansu Province and State Key Laboratory of Applied Organic Chemistry Lanzhou University Gansu, Lanzhou, 730000 (P.R. China) Lanzhou University, Lanzhou 730000, P.R. China.

E-mail: wangbd@lzu.edu.cn

1. Experimental Section.

1.1 Chemicals and Materials: Iron (III) acetylacetonate (99.9%), copper (II) acetylacetonateoleic, oleylamine (70%), diphenyl ether and 4-Methyl-o-phenylenylenediamine were purchased from Sigma Aldrich. Graphite powder (40 nm, 99%), 3,4-dihydroxybenzaldehyde, sarcosine (99%), 4-dimethylaminopyridine (99%), Cs_2CO_3, 2-Ethynylthiophene (97%), 1-Heptyne (97%), 3,3-Dimethyl-1-butyne (95%), 1-Ethynyl-4-fluorobenzene (98%), 4-Methoxyphenylacetylene (99%), o-phenylenediamine (98%), 4-Ethynyltoluene (98%) and phenylacetylene were purchased from Aladdin. 4-Nitro-o-phenylenediamine (98%) and 4-Bromo-o-1,2-benzenediamine (97%) were purchased from J&K, 4-Methoxy-o-phenylenediamine (98%) were purchased from Alfa Aesar. GO and rGO were prepared according to the published method.[1]

1.2 Synthesis of Core-shell Fe_3O_4@Cu_2O NCs: $Fe(acac)_3$ (2 mmol), $Cu(acac)_2$ (1 mmol), oleylamine (15 mL) and diphenyl ether (15 mL) were mixed and magnetically stirred under a flow of nitrogen. The reaction mixture was dehydrated at 110 ^{0}C for 1.5 h under a blanket of N_2, then heated to 265 ^{0}C, and aged at this temperature for 1 h. After the reaction, the solution was allowed to cool down to room temperature. The core-shell Fe_3O_4@Cu_2O NCs were precipitated upon the addition of 50 mL of ethanol and centrifuging. In order to remove the excess oleylamine on the surface of NCs, the NCs were washed by petroleum ether and ethanol mixed solution. Finally, the product was dispersed in chloroform.

1.3 Synthesis of 6 nm $CuFe_2O_4$ NPs NPs: 2 mmol of $Fe(acac)_3$ and 1 mmol of $Cu(acac)_2$ were dissolved in 10 mL of oleylamine and 15 mL dibenzyl. The reaction mixture was dehydrated at 110 ^{0}C for 1.5 h under N_2 atmosphere, then heated to 300 ^{0}C, and aged at this temperature for 2 h. After the reaction, the solution was allowed to cool down to room temperature. The $CuFe_2O_4$ NPs were precipitated upon the addition of 50 mL of ethyl alcohol and centrifuging. In order to remove the excess oleylamine on the surface of NPs, the NPs were washed by petroleum ether and ethanol mixed solution. Finally, the product was dispersed in chloroform.

1.4 Synthesis of GO: GO was made by a modified Hummer's method with a little modification[2]: Graphite powder (1.00 g) was grounded with NaCl (20.00 g) for 30 min. Afterward, NaCl was washed away using water. Then the graphite was heated at 60 ℃ in oven for 24 h to remove any water. The dried solid was then mixed with 50 mL of concentrated sulfuric acid in a 250 mL round-bottom flask. Next, 1.00 g of $NaNO_3$ was added to the mixture. The flask was then placed in an ice bath, and 6.00 g of $KMnO_4$ was slowly added while the temperature was kept below 5 ℃ for 0.5 h, and then stirred at room temperature for 48 h, afterward, 80 mL of water was slowly added to the flask, and keep the temperature at 5 ℃ for 20 min in an ice bath. Twenty minutes later another 80 mL of water was added. After 20 min, 120 mL of water was added. Afterward, 6 mL of 30% H_2O_2 was added to the flask under stirring. This suspension was stirred at room temperature for 2 h. After 2 h, the suspension was centrifuged at low speed (6000 rpm, 5 min) and washed with ultrapure water for 3 times. The obtained suspension was dispersed in optimum ultrapure water, and the water was removed by freeze drier.

1.5 Synthesis of rGO: For the synthesis of rGO[3], 20 mg prepared GO was dispersed in 20 mL ultrapure water after 30 min of ultrasoic treatment. 11.4 mg $NaBH_4$ was slowly added to the system and stirred at room temperature for 3h. Then defined amount of HCl (0.1 M) was added to the system dropwise. The product was centrifuged and washed by ethanol three times. The solid product was vacuum-dried overnight at room temperature.

1.6 Synthesis of rGO-S-DIB[4]: rGO (10 mg) was dispersed in 10 mL pyridine and 50 ml DMF mixture solution by ultrasonic affording a stable gray dispersion. An excess of N-methyl-glycine (50 mg) and 3,

4-dihydroxybenzaldehyde (50 mg) were added to the above dispersion system and the mixture was refluxed at 145 ℃ for 96 h. The products were precipitated upon the addition of 35 mL of petroleum. The suspension was centrifuged at low speed (6000 rpm, 3 min) and washed with ethanol and petroleum three times. Finally, the rGO-S-DIB was dispersed in ethanol (10 mL).

1.7 Synthesis of Fe_3O_4@Cu_2O-rGO nanocomposite: 10 mL rGO-S-DIB was added into 100 mL round-bottom flask, and then another 40 mL ethanol was added under ultrasonication. Fe_3O_4@Cu_2O NCs (4 mg) in 5 mL chloroform was added into above dispersion solution and stirred overnight at room temperature 24 hour. The product was precipitated by adding hexane and collected by exogenous magnet. The resulting Fe_3O_4@Cu_2O-rGO nanocomposite was washed with hexane three times and was dispersed in ethyl alcohol.

1.8 Surface Area and Pore Size: Surface areas of samples were determined using the Brunauer-Emmett-Teller (BET) principle, and the pore parameters of the samples were determined with the Barrett-Joyner-Halenda (BJH) method, derived from N_2 adsorption-desorption measurements carried out using an automatic micropore physisorption analyzer (Micromeritics TriStar II 3020, U.S.A.) at 77 K. Prior to analysis, samples were degassed in situ at 100 ^{0}C for 8 h.

1.9 General procedure for the Fe_3O_4@Cu_2O-rGO nanocomposite-catalyzed cyclization reaction: O-phenylenediamine (27.0 mg, 0.25mmol), Fe_3O_4@Cu_2O-rGO nanocomposite (5.0 mg, 1 mol%), DMAP (92.55 mg, 0.75mmol), Cs_2CO_3 (244.48 mg, 0.75mmol), phenylacetylene (1 mmol) and toluene(2 ml) were added to a flask with a magnetic stirrer bar. The reaction mixture was stirred for 8 h at 70 ℃. After cooling to room temperature, catalyst was recycled by magnet and the palm red mixed liquid was diluted with ethyl acetate. The solvent was removed by the rotary evaporator to get the crude product, which was further purified by silica gel chromatography (petroleum/ethyl acetate = 10/1 as eluent) to yield corresponding product. The identity of the products was confirmed by ^{1}H and ^{13}C NMR spectroscopic analysis.

1.10 The characterization of core-shell Fe_3O_4@Cu_2O NCs and Fe_3O_4@Cu_2O-rGO nanocomposite.: As shown in Figure S1, the energy-dispersive X-ray (EDX) analysis on selected different areas of an

individual Fe_3O_4@Cu_2O sphere demonstrates clearly that the core-shell spheres contain Cu, O and Fe elements. The valence state of Cu, O and Fe elements in the core-shell Fe_3O_4@Cu_2O nanocomposite is determined by X-ray photoelectron spectra (XPS). As shown in Figure S2 the elements Cu, Fe, O, and C can be observed clearly. The low intensity of the Fe 2p peaks is due to the Cu_2O coating layer. The appearance of C 1s and N 1s peaks can be ascribed to the absorbed or bonded oleylamine. The high-resolution XPS spectrum displayed Fe 2p doublet at 711.7 and 725.3 eV (Figure S1d) correspond to Fe $2p_{3/2}$ and Fe$2p_{1/2}$, respectively, which are in good agreement with the known values of Fe $2p_{3/2}$ and Fe $2p_{1/2}$ of Fe_3O_4, respectively.[5] One can see from Figure S2e that the high-resolution XPS spectrum of Cu 2p shows that Cu is in the +1 oxidization state in the product. The binding energy of Cu $2p_{3/2}$ and Cu $2p_{1/2}$ are 933.8 and 953.9 eV, which is in conformity with the results reported elsewhere.[6] In addition, O 1s core level peak, centered at 530.5 eV displayed in Figure S2c, belongs to the O^{2-} contribution. In addition to the detailed TEM analysis, the crystal structure of these core-shell Fe_3O_4@Cu_2O nanoparticles was studied by powder X-ray diffraction (XRD). The XRD patterns (Figure 2A) showed the two mixed phases of cubic Fe_3O_4 (JCPDS card no. 17-0320) and tetragonal Cu_2O (JCPDS card no. 080-1268). No other crystalline impurities are detected, suggesting that the compositions of the above structures are Fe_3O_4 and Cu_2O. Compared with spherical $CuFe_2O_4$ NPs (Figure S9) , relatively strong reflection peaks for Cu_2O but weak peaks for Fe_3O_4, reflecting their core-shell structure (Figure S9). In the FT-IR spectrum, the absorption peak of phenolic υ(C–O) vibration in rGO-S-DIB is observed at 1174 cm^{-1}. After forming Fe_3O_4@Cu_2O-rGO nanocomposite, the peak of the phenolic υ(C–O) at 1174 cm^{-1} is not observed. However, a new absorption peak of C–O–Cu vibration at 1095 cm^{-1} appears, indicating that the phenolic hydroxyl group of rGO-S-DIB are bound to the surface of Fe_3O_4@Cu_2O NCs (Figure S7).[7,8]

1.11 The formation mechanism of core-shell Fe_3O_4@Cu_2O NPs: to gain an insight into the formation mechanism of core-shell Fe_3O_4@Cu_2O NPs, the growth process was traced with reaction time. Figure S3 gives the TEM images of the intermediate products observed at different reaction times at 265 ^{0}C to follow the reaction progress. The Fe_3O_4 NPs were firstly formed when iron (III) and copper (II) acetylacetonate ($Fe(acac)_3$ and $Cu(acac)_2$) solution was heated to 265 ^{0}C in the presence of diphenyl ether

(Figure S3a-e). The $Cu(acac)_2$ was gradually decomposed and preferentially deposited on the preformed Fe_3O_4 NPs with the reaction time increasing from 20 min to 60 min, which revealed that the formation of core-shell Fe_3O_4@Cu_2O NCs was slightly relevant to the aging time. The TEM image taken after 60 min of reaction shows that the almost all NPs are formed core-shell nanocrystal. The observed shape evolution provides strong evidence that the shell growth process partially follows the Ostwald ripening mechanism.[9] Due to the surface plasmon resonance, the UV absorption peak of Fe_3O_4@Cu_2O NCs is at 576 nm (Figure S4). Time-dependent UV-vis absorption spectra (Figure S5) shows increasing of the characteristic absorption at 576 nm, and the absorption intensity reaches the maximum value at 60 min. After that time, the absorption intensity decreases. Both TEM images and UV-vis absorption spectra demonstrated that Cu_2O layer gradually deposited on the surface of Fe_3O_4 NPs, and all the core-shell structure nanoparticles formed completely in sixty minutes. The increased ratio of $n_{Cu}/(n_{Fe}+n_{Cu})$ of as-prepared nanocrystals with increasing time using inductively coupled plasma atomic emission spectroscopy (ICP) further inferred the core-shell structure (Figure S3f). Based above analysis, the formation mechanism was showed in Scheme 2.

1.12 Solvent selection: To search for a suitable solvent, o-phenylenediamine and phenylacetylene were used as model substrates (Table S1). Among the solvents tested, toluene was the most effective reaction solvent for this reaction (Table S1, entry 4). Other solvents afforded the products in low yields (Table S1, entries 1-3 and 5-8). Also, we found that this reaction could not work only in the presence of organic base (Table S2, entry 4). In the organic base containg DMAP, Pyridine and Et_3N, only the DMAP get the best yield (Table S2, entry 3 and 7). Among inorganic bases tested, Cs_2CO_3 turned out to be the best (Table S2, entry 7).

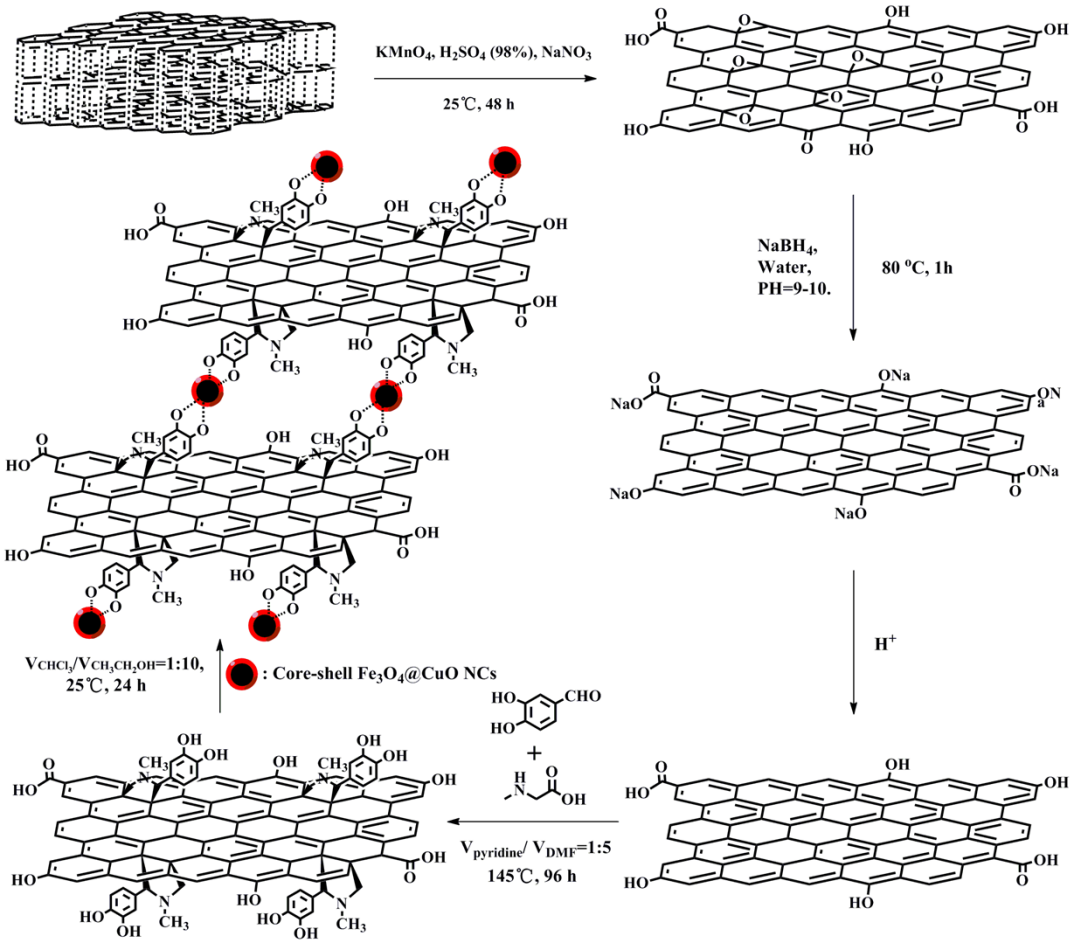

Scheme S1. Synthetic route of Fe_3O_4@Cu_2O-rGO nanocomposite.

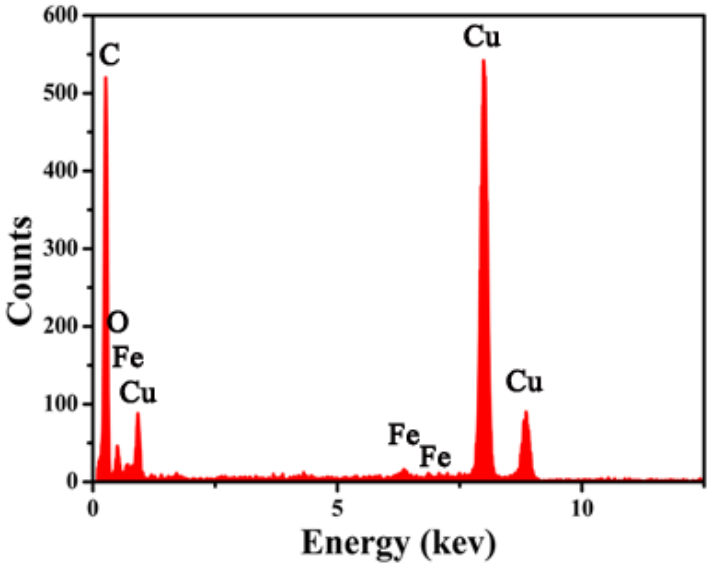

Figure S1. EDX pattern of Fe_3O_4@Cu_2O NCs.

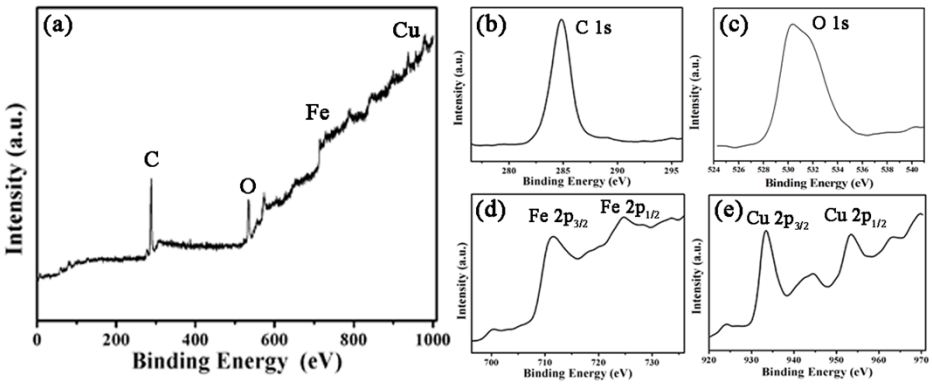

Figure S2. (a) XPS spectra of Fe_3O_4@Cu_2O NCs; (b) The spectrum in the C 1s region; (c) The spectrum in the O 1s region; (d) The spectrum in the Fe $2p_{3/2}$ and Fe $2p_{1/2}$; (e) The spectrum in the Cu $2p_{3/2}$ and Cu $2p_{1/2}$.

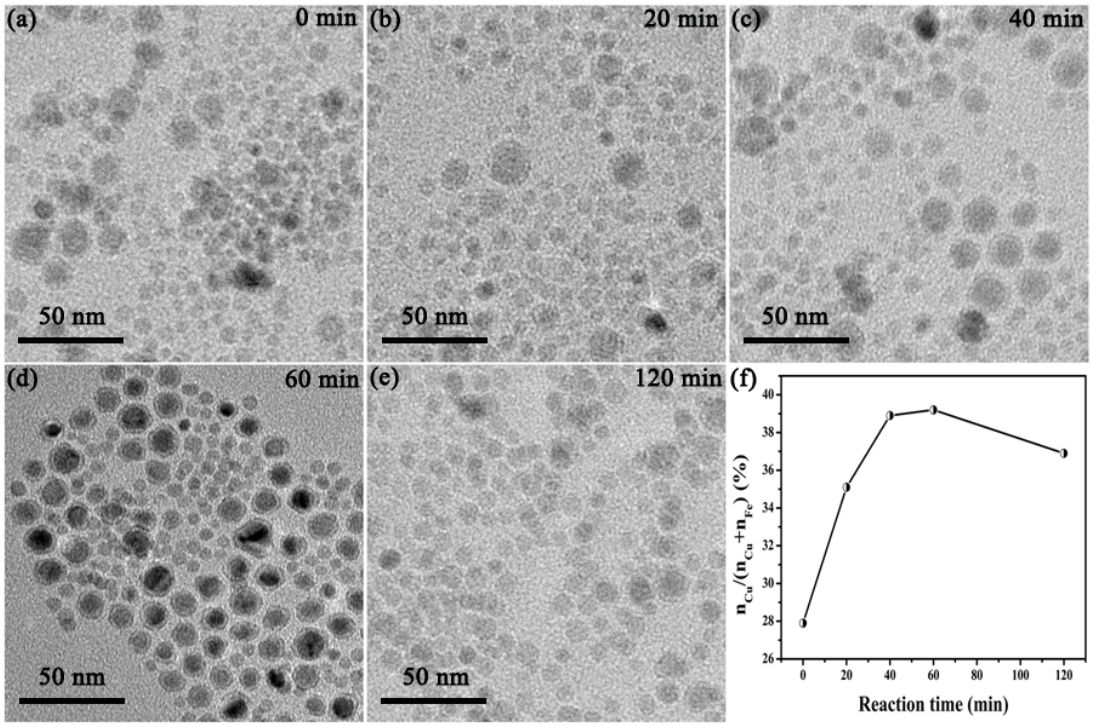

Figure S3. TEM image of the obtained nanocrystals after reaction with (a) 0 min, (b) 20 min, (c) 40 min, (d) 60 min and (e) 120 min at 265 ^oC in the flask; (f) The image of the changing of $n_{Cu}/ (n_{Cu} + n_{Fe})$ of the obtained nanocrystals after reaction with 0 min, 20 min, 40 min, 60 min and 120 min at 265 ^oC in the flask through the measurement by ICP.

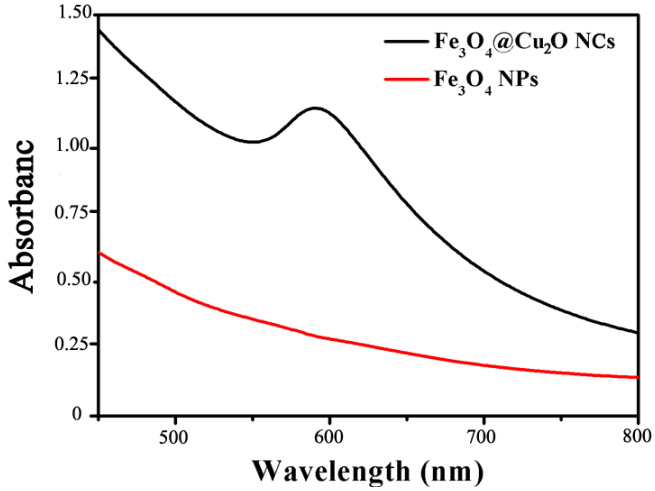

Figure S4. UV-Vis spectra of Fe_3O_4@Cu_2O NCs (black line) and Fe_3O_4 NPs (red line).

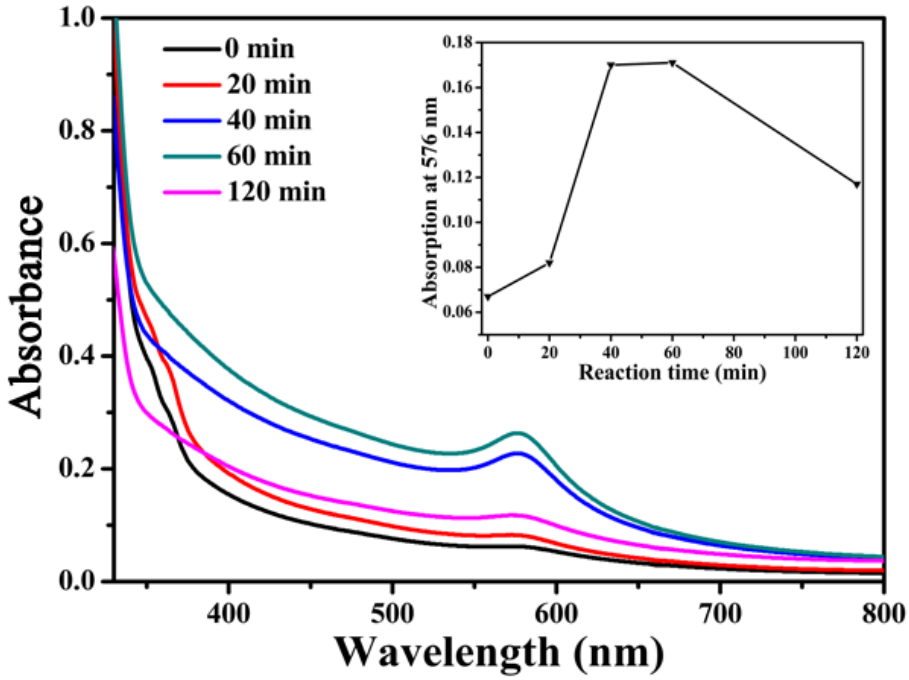

Figure S5. UV-Vis spectra of the obtained nanocrystals after reaction with 0 min, 20 min, 40 min, 60 min and 120 min at 265 °C.The inset shows the UV-Vis spectra absorb intensity change of the obtained nanocrystals after reaction with 0 min, 20 min, 40 min, 60 min and 120 min at 576 nm.

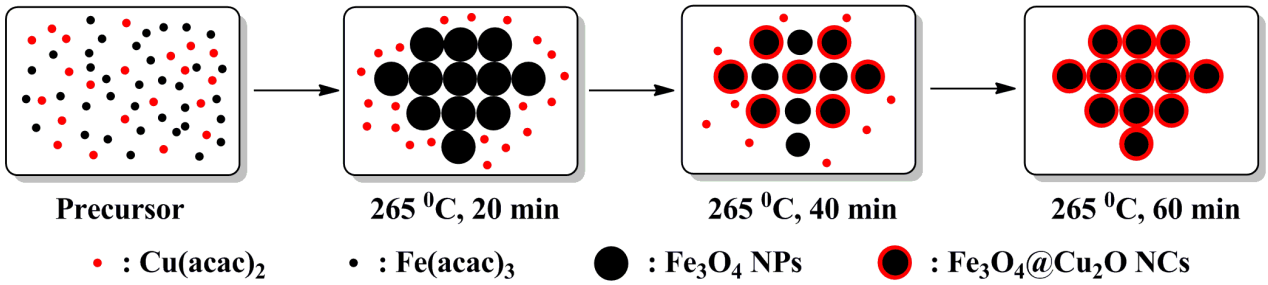

Scheme S2. A schematic illumination for the forming process of core-shell Fe_3O_4@Cu_2O NCs.

Figure S6. TEM images of rGO-S-DIB,

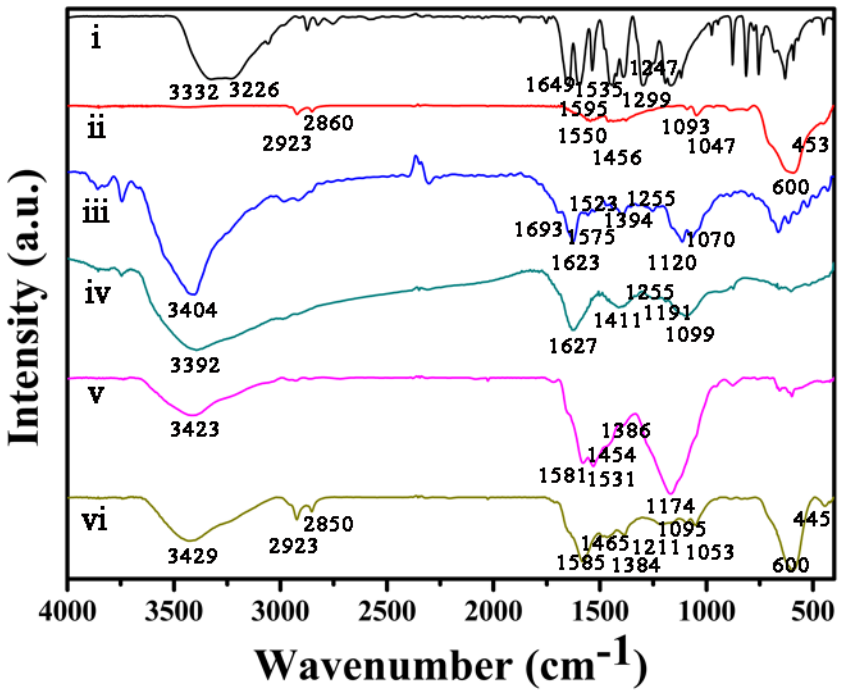

Figure. S7. FTIR spectra of i: 3,4-Dihydroxybenzaldehyde, ii: Fe_3O_4@Cu_2O NCs, iii: as-synthesized GO, iv: rGO, v: rGO-S-DIB and vi: Fe_3O_4@Cu_2O-rGO nanocomposities.

Figure S8. Magnetic behavior of Fe_3O_4@Cu_2O NCs (black line) and Fe_3O_4@Cu_2O-rGO nanocompositie (red line) at 300 K. The photographs demonstrate that Fe_3O_4@Cu_2O-rGO nanocompositie in toluene can be attracted and arranged vertically by a magnetic bar.

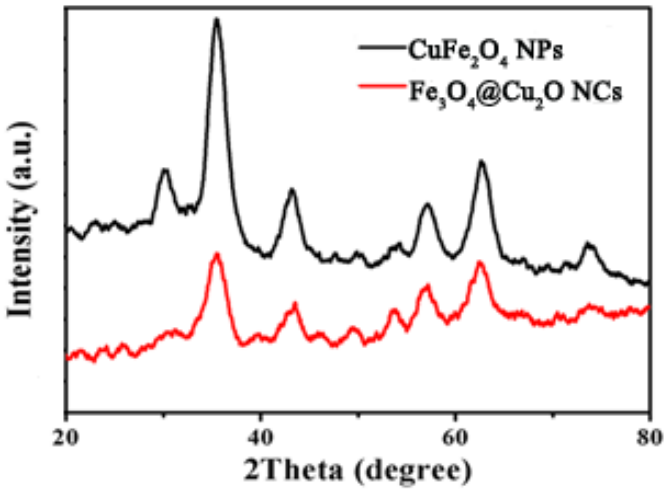

Figure S9. XRD pattern of $CuFe_2O_4$ NPs and Fe_3O_4@Cu_2O NCs.

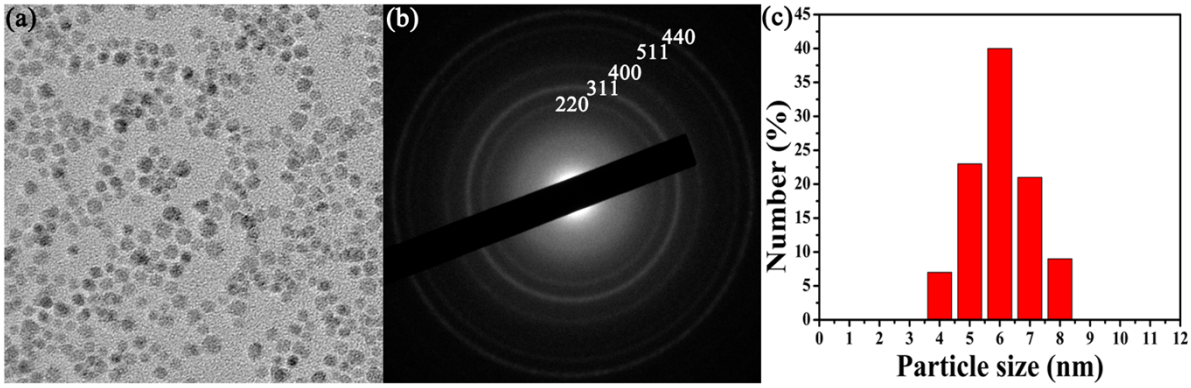

Figure S10. (A) TEM image of $CuFe_2O_4$ NPs; (B) The selected area electron diffraction (SAED) pattern acquired from $CuFe_2O_4$ NPs; (C) The size distribution histograms of $CuFe_2O_4$ NPs.

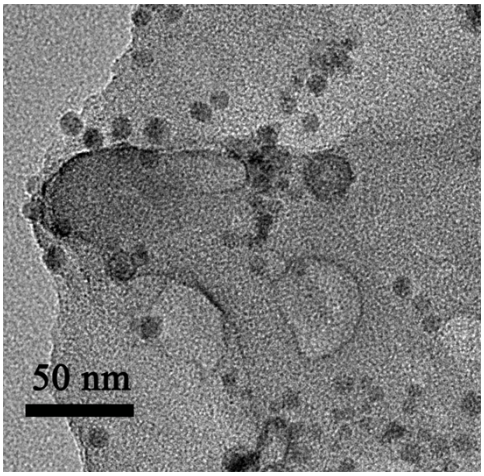

Figure S11. TEM image of Fe_3O_4@Cu_2O-rGO nanocomposite after reusing 9 times.

Table S1. Screening of solution for synthesis of quinoxalines with o-phenylenediamine and phenylacetylene [a)].

Entry	Solution	Yield [b)] (%)
1	N, N-Dimethylformamide	45
2	Tetrahydrofuran	30
3	Pyridine	75
4	Toluene	92
5	Ethanol	40
6	Ethyl acetate	65
7	Acetonitrile	47
8	Distilled water	35

[a] All of the reactions were carried out in sealed tubes using 0.25 mmol of 1, 1 mmol of 2, 1 mol% of Fe_3O_4@Cu_2O-rGO, and 3 equiv of each base in toluene at 70 ℃ for 8 h. [b] Isolated yields.

Table S2. Screening of base for synthesis of quinoxalines with o-phenylenediamine and phenylacetylene [a].

Entry	Base	Yield [b] (%)
1	K_2CO_3，Et_3N	60
2	K_2CO_3，Pyridine	65
3	K_2CO_3，DMAP	70
4	DMAP	0
5	Cs_2CO_3，Et_3N	70
6	Cs_2CO_3，Pyridine	75
7	Cs_2CO_3，DMAP	92

[a] All of the reactions were carried out in sealed tubes using 0.25 mmol of 1, 1 mmol of 2, 1 mol% of Fe_3O_4@Cu_2O-rGO, and 3 equiv of each base in toluene at 70 ℃ for 8 h. [b] Isolated yields.

Table S3. Using various catalys for synthesis of quinoxalines with o-phenylenediamine and phenylacetylene [a].

Entry	Catalyst	Yield [b] (%)
1	Fe_3O_4@Cu_2O-rGO	92
2	Fe_3O_4@Cu_2O NCs	88
3	rGO	Trace
4	Fe_3O_4 NPs	Trace
5	$Cu(OAc)_2 \cdot H_2O$	86
6	$Cu(OTf)_2$	70
7	$CuCl_2$	29
8	—	Trace

a) All of the reactions were carried out in sealed tubes using 0.25 mmol of 1, 1 mmol of 2, 1 mol% of Fe_3O_4@Cu_2O-rGO, and 3 equiv of each base in toluene at 70 ℃ for 8 h. **b)** Isolated yields.

Table S4. Catalytic cycle efficiency of $Cu(OAc)_2 \cdot H_2O$, Fe_3O_4@Cu_2O NCs and Fe_3O_4@Cu_2O-rGO nanocomposite.

	$Cu(OAc)_2 \cdot H_2O$	Fe_3O_4@Cu_2O NCs	Fe_3O_4@Cu_2O-rGO nanocomposite
1	86	88	90
2	0	83	89
3	0	80	89
4	0	60	89
5	0	0	88
6	0	0	87

7	0	0	87
8	0	0	86
9	0	0	86

2. Product Charaterization.

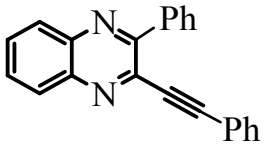

2-phenyl-3-(phenylethynyl)quinoxalne: light yellow solid; m.p 109-111 ^{o}C; ^{1}H NMR (400 MHz, $CDCl_3$): δ 8.15-8.09(m, 4H), 7.79-7.75 (m, 2H), 7.59-7.54 (m, 3H), 7.50-7.47 (m, 2H), 7.38-7.32 (m, 3H); ^{13}C NMR (100 MHz, $CDCl_3$): δ 155.22, 141.12, 140.83, 138.20, 137.74, 132.23, 130.80, 130.42, 129.80, 129.72, 129.42, 128.87, 128.56, 128.27, 121.79, 95.17, 88.45.

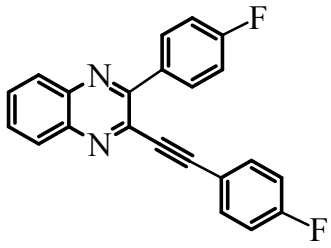

2-(4-flurophenyl)-3-((4-flurophenyl)ethynyl) quinoxaline: white solid; m.p 212-218 ^{o}C; ^{1}H NMR (400 MHz, $CDCl_3$): δ8.15-8.10 (m, 4H), δ7.80 (q, J=3.0Hz, 2H), δ7.49 (q, J=5.7, 2H), δ7.26 (t, J=8.4,2H), δ7.07 (t, J=8.4,2H); ^{13}C NMR (100 MHz, $CDCl_3$): δ153.87, 141.02, 140.69, 134.23, 134.15, 131.79, 131.71, 130.92, 130.50, 129.27, 128.78, 117.67, 116.17, 115.94, 115.39, 115.17, 94.00, 87.94.

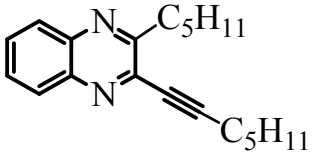

2-(butyl)-3-(hex-1-yn-1-yl) quinoxaline: colorless less liquid, ^{1}H NMR (400 MHz, $CDCl_3$): δ8.01 (dd, J=6.3Hz, J=10.2Hz, 2H), 7.69 (dd, J=6.3Hz, J=10.5Hz, 2H), 3.16 (t, J=7.5Hz, 2H), 2.57 (t, J=7.2Hz, 2H), 1.90-1.82 (m, 2H), 1.74-1.67 (m, 2H), 1.63-1.45 (m, 4H), 0.96-0.91(m, 6H); ^{13}C NMR (100 MHz, $CDCl_3$): δ158.90, 140.77, 140.58, 140.03, 130.02, 129.36, 128.74, 128.56, 97.53, 78.72, 36,58, 31.98, 31.29, 22.61, 22.32, 19.76, 14.14, 14.07.

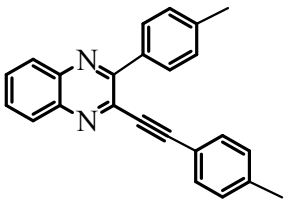

2-(p-tolyl)-3-(p-tolylethynyl)quinoxaline: light yellow solid; m.p 112-114 ^{o}C; ^{1}H NMR (400 MHz, $CDCl_3$): δ8.14-8.10 (m, 2H), 8.05 (d, J=8.1Hz, 2H), 7.78-7.74 (m, 2H), 7.43 (d, J=8.4Hz, 2H), 7.36 (d, J=7.5Hz, 2H), 7.16 (d, J=7.5Hz, 2H), 2.48 (s, 3H), 2.38 (s, 3H); ^{13}C NMR (100 MHz, $CDCl_3$): δ155.01, 140.97, 140.81, 140.13, 139.95, 138.27, 134.88, 132.15, 130.60, 130.18, 129.74, 129.35, 128.96, 128.77, 118.78, 95.40, 88.16, 21.79, 21.62.

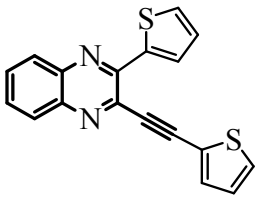

2-(thiophen-2-yl)-3-(thiophen-2-ylethynyl) quinoxaline: light yellow solid; m.p 94-96 ^{o}C; ^{1}H NMR (400 MHz, $CDCl_3$): δ8.43 (d, J=1.8Hz, 1H), 8.09-8.02 (m, 2H), 8.01 (d, J=4,2Hz, 1H), 7.76-7.71 (m, 3H), 7.47 (dd, J=3.0Hz, J=5.4Hz, 1H), 7.35 (dd, J=3.0Hz, J=4.8Hz, 1H), 7.28(d, J=5.1Hz, 1H); ^{13}C NMR (100 MHz, $CDCl_3$): δ147.59, 141.91, 139.17, 139.12, 132.54, 130.28, 129.81, 129.67, 129.50, 128.50, 128.23, 128.12, 127.60, 127.50, 121.80, 92.49, 88.98.

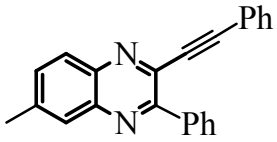

6-methyl-2-phenyl-3-(phenylethynyl)quinoxaline: Light yellow solid; m.p 140-142 ^{o}C; ^{1}H NMR (400 MHz, $CDCl_3$): δ8.10-8.07 (m, 2H), 8.02 (d, J=9.0Hz, 1H), 7.90 (s, 1H), 7.61-7.56(m, 4H), 7.50-7.47 (m, 2H), 7.38-7.31 (m, 3H), 2.60 (S, 3H). ^{13}C NMR (100 MHz, $CDCl_3$): δ155.05, 141.53, 141.07, 140.97, 139.23, 137.89, 137.75, 133.10, 132.71, 132.10, 132.06, 129.69, 130.23, 129.67, 129.63, 129.56, 129.54, 129.49, 128.80, 128.64, 128.49, 128.38, 128.32, 127.74, 121.80, 95.01, 88.73, 22.03, 21.97.

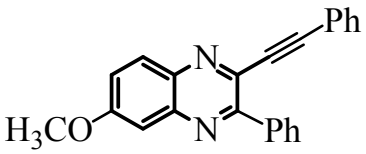

6-methoxy-2-phenyl-3-(phenylethynyl)quinoxaline: light yellow solid; m.p 150-152 °C; ^{1}H NMR (400 MHz, $CDCl_3$): δ8.10-8.06 (m, 2H), 8.01(d, J=9.9Hz, 1H), 7.58-7.53 (m, 2H), 7.51-7.47 (m, 2H), 7.44-7.39 (m, 2H), 7.39-7.35 (m, 2H), 7.35-7.32 (m, 2H). ^{13}C NMR (100 MHz, $CDCl_3$): δ161.20, 152.87, 142.67, 137.90, 137.11, 132.20, 132.17, 130.32, 129.70, 129.63, 129.49, 128.56, 128.24, 124.27, 121.90, 105.98, 94.86, 88.52, 55.97.

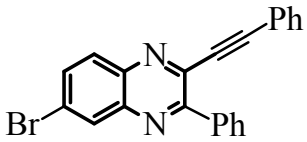

6-bromo-2-phenyl-3-(phenylethynyl)quinoxaline: Light yellow solid; m.p 150-152 °C; ^{1}H NMR (400 MHz, $CDCl_3$): δ8.32-8.30 (m, 1H), 8.09 (dd, J=1.8Hz, J=8.1Hz, 2H), 8.00 (d, J=8.7Hz, 1H), 7.85 (t, J=2.4Hz, 1H), 7.60-7.56 (m, 3H), 7.49 (d, J=7.8Hz, 2H), 7.41-7.34 (m, 3H). ^{13}C NMR (100 MHz, $CDCl_3$): δ161.20, 152.87, 142.67, 137.90.22, 137.85, 137.11, 132.20, 132.06, 130.32, 129.70, 129.63, 129.49, 128.56, 128.24, 124.27, 121.90, 105.98, 94.86, 88.53, 56.03, 55.97.

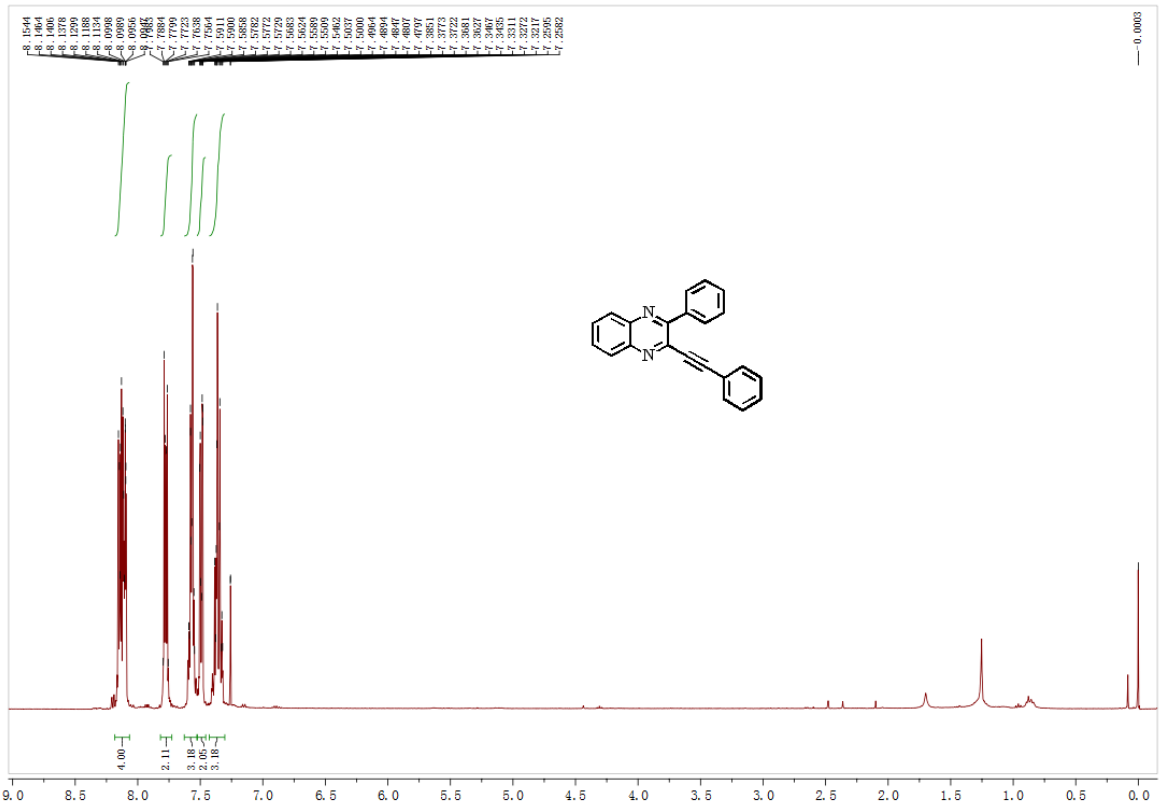

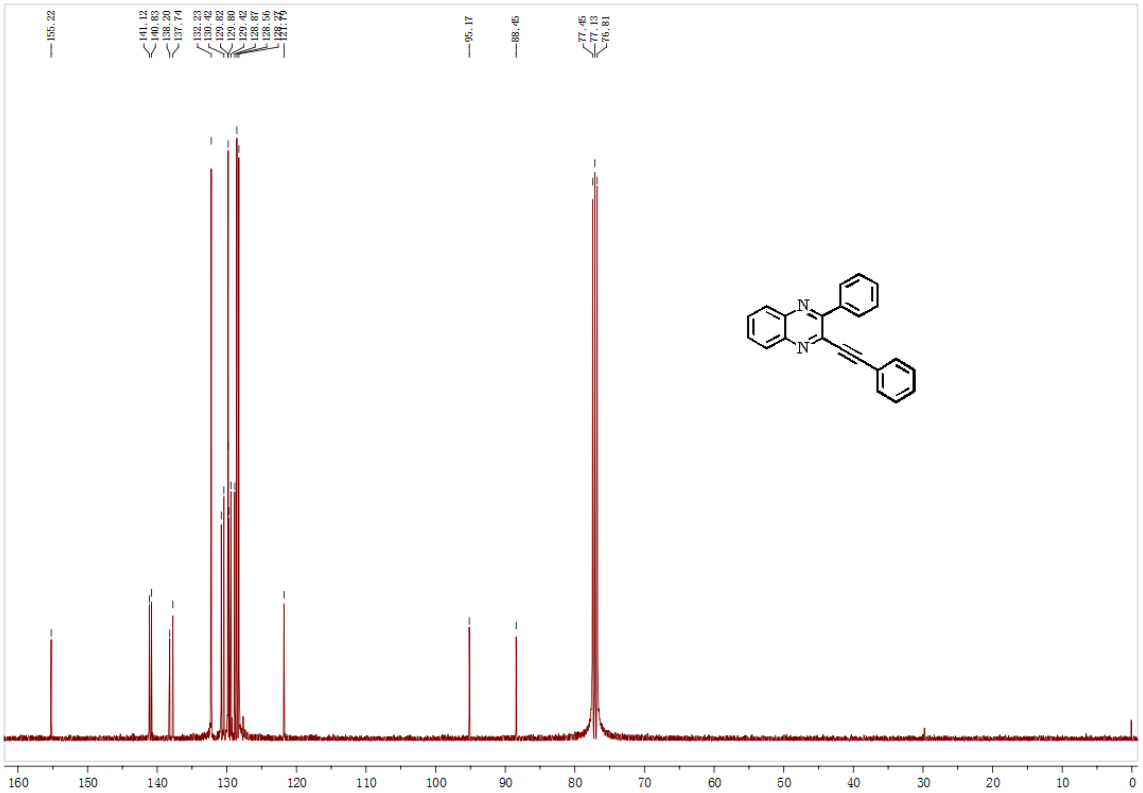
155.22
141.12
140.83
138.20
137.74
132.23
130.42
129.82
129.80
129.42
128.87
128.56
121.79
95.17
88.45
77.45
77.13
76.81
N
N
160
150
140
130
120
110
100
90
80
70
60
50
40
30
20
10
0

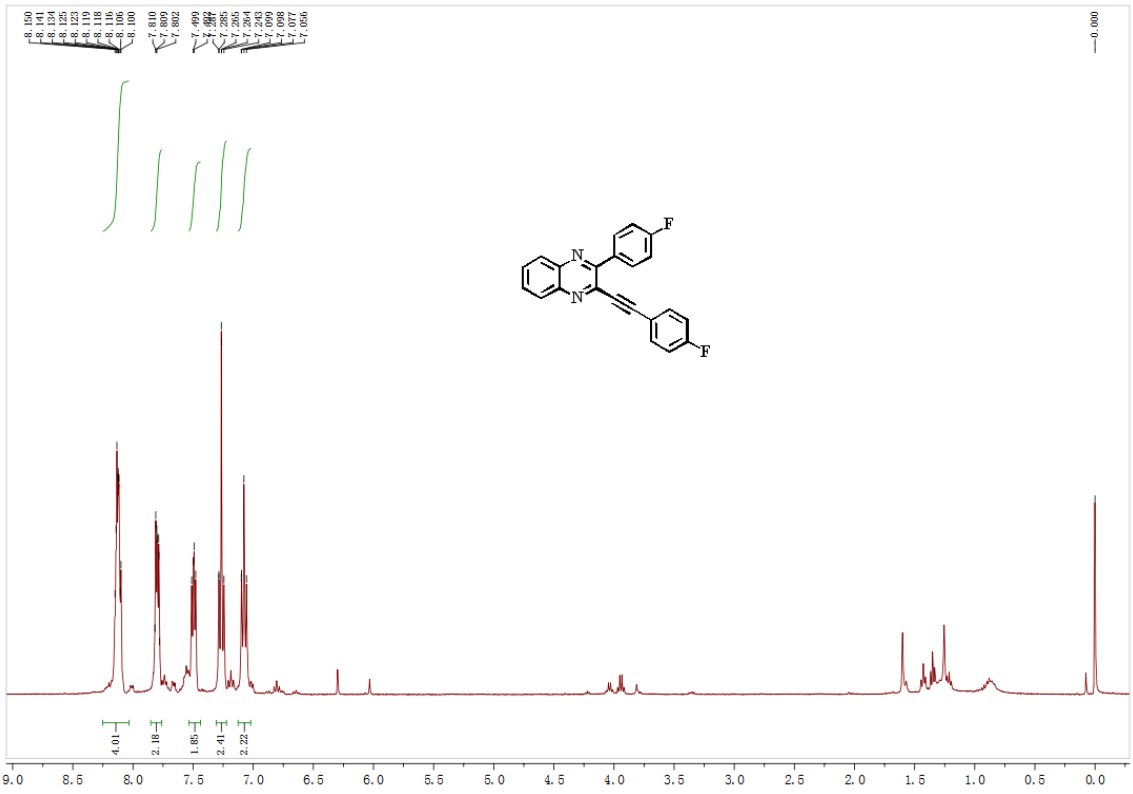
8.150
8.141
8.134
8.125
8.123
8.119
8.118
8.116
8.111
8.106
8.100
7.810
7.809
7.802
7.499
7.285
7.265
7.264
7.243
7.099
7.098
7.077
7.056
0.000
F
F
N
N
4.01
2.18
1.85
2.41
2.22
9.0
8.5
8.0
7.5
7.0
6.5
6.0
5.5
5.0
4.5
4.0
3.5
3.0
2.5
2.0
1.5
1.0
0.5
0.0

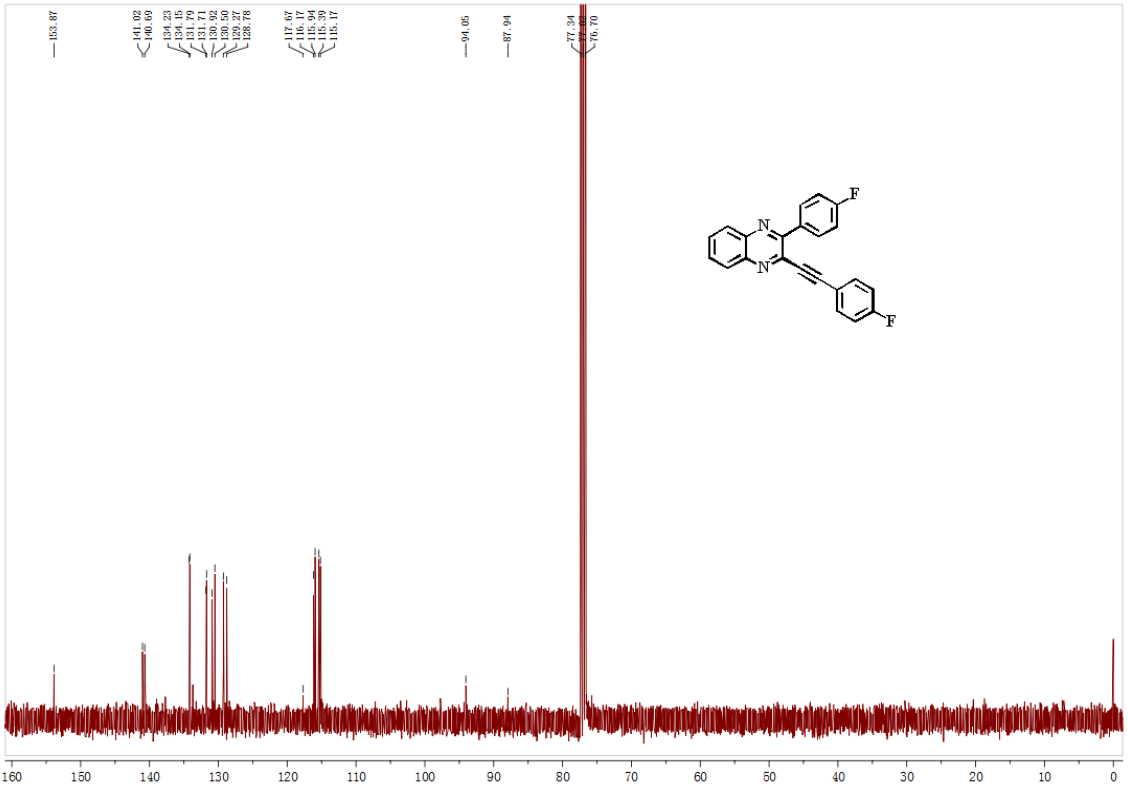
153.87
141.02
140.69
134.23
134.15
131.79
131.71
130.92
130.50
129.27
128.78
117.67
116.17
115.94
115.39
115.17
94.05
87.94
77.34
77.02
76.70
F
F
N
N

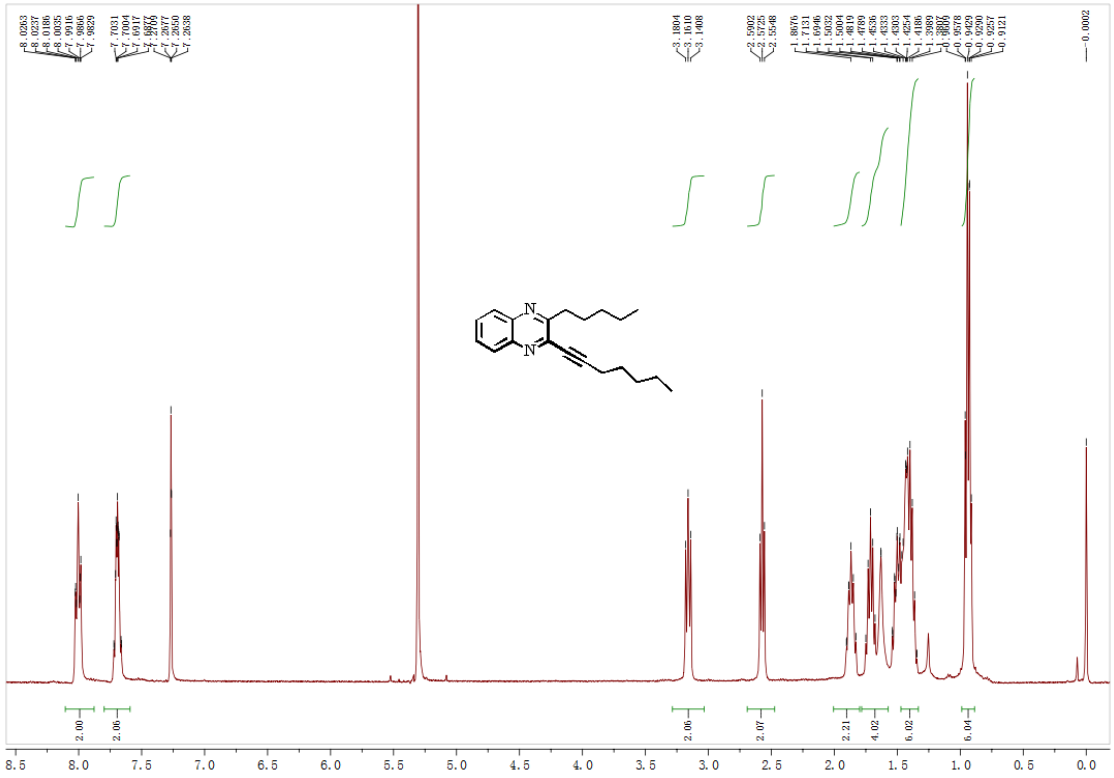
8.0263
8.0237
8.0186
8.0095
7.9916
7.9866
7.9829
7.7031
7.7004
7.6917
7.2677
7.2650
7.2638
3.1804
3.1610
3.1408
2.5902
2.5725
2.3548
1.8076
1.7131
1.6946
1.5932
1.5004
1.4819
1.4789
1.4536
1.4253
1.4033
1.4254
1.4186
1.3989
0.9578
0.9459
0.9360
0.9257
0.9121
0.0002
N
N
2.00
2.06
2.06
2.07
2.21
4.02
6.02
6.04

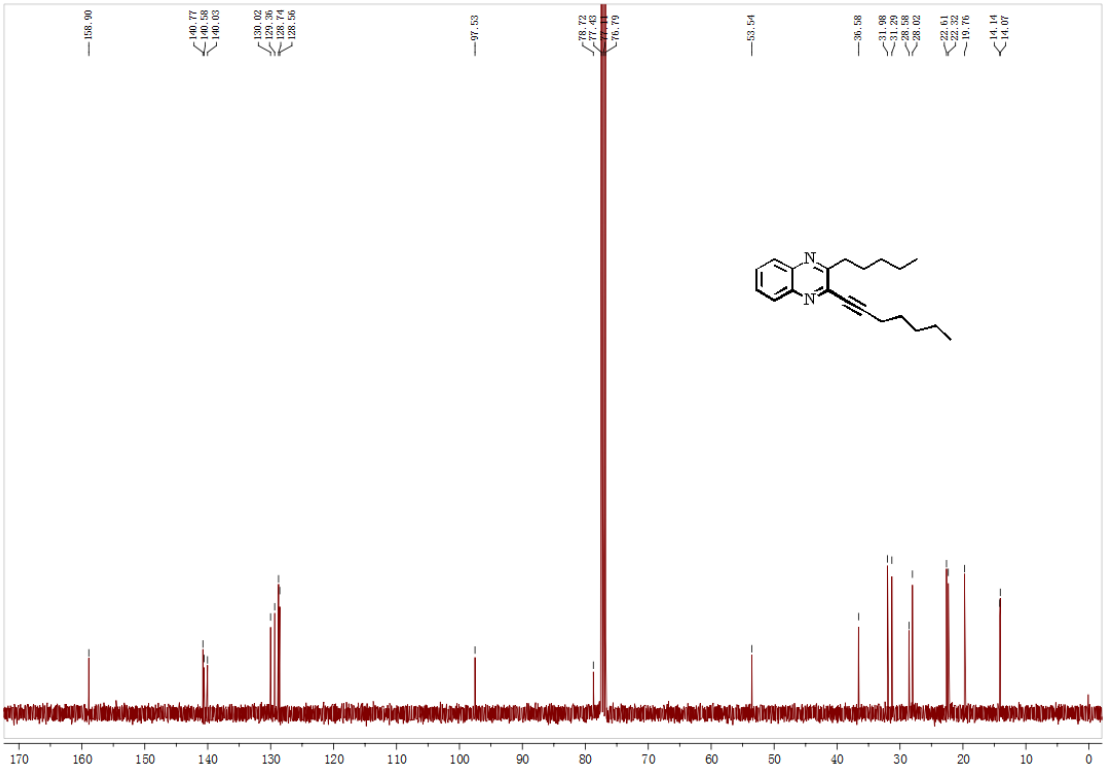
158.90
140.77
140.58
140.03
130.02
129.36
128.74
128.56
97.53
78.72
77.43
77.11
76.79
53.54
36.58
31.98
31.29
28.58
28.02
22.61
22.32
19.76
14.14
14.07
N
N

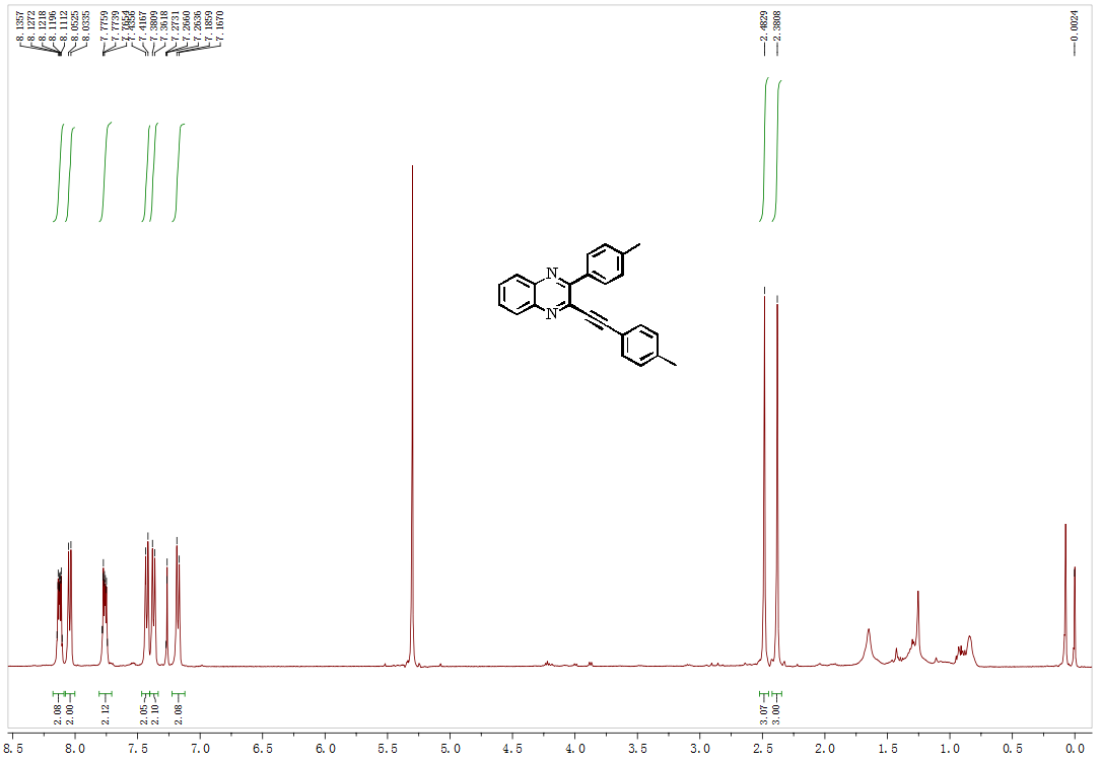
8.1357
8.1272
8.1218
8.1196
8.1112
8.0525
8.0335
7.7759
7.7739
7.4167
7.3809
7.3618
7.2771
7.2660
7.2636
7.1859
7.1670
2.4829
2.3808
0.0024
N
N
2.08
2.00
2.12
2.05
2.10
2.08
3.07
3.00

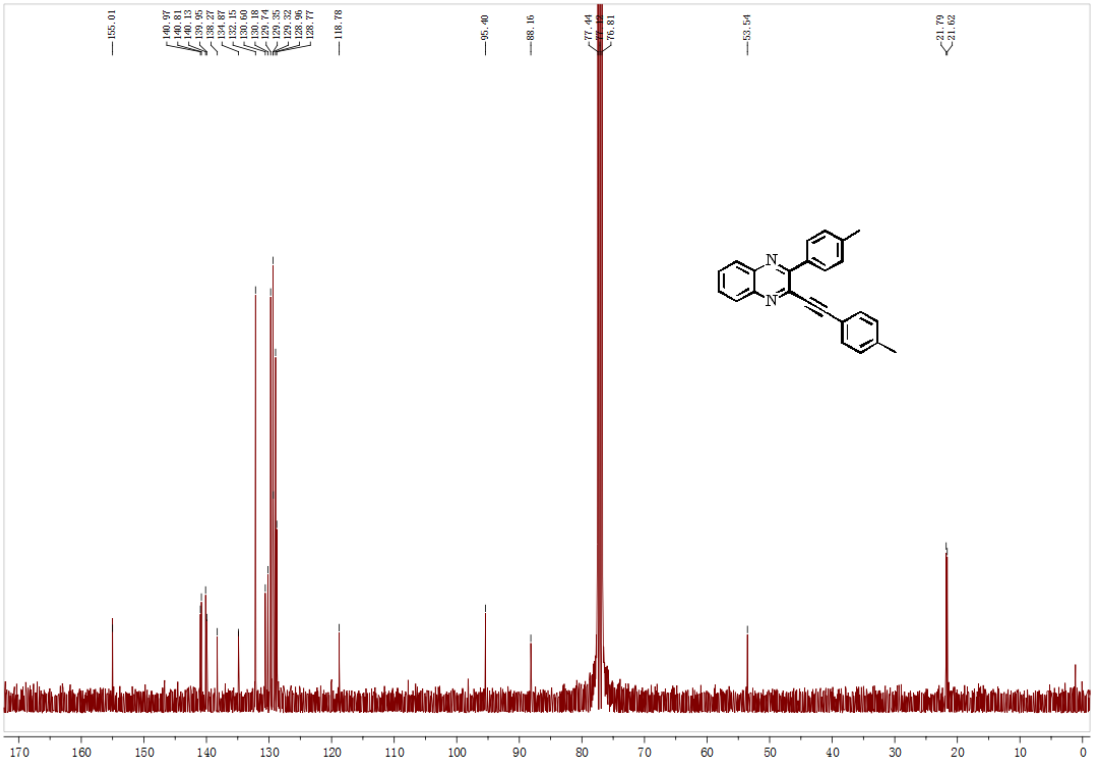
155.01
140.97
140.81
140.13
139.95
138.27
134.87
132.15
130.60
130.18
129.74
129.35
129.32
128.96
128.77
118.78
95.40
88.16
77.44
76.81
53.54
21.79
21.62
170
160
150
140
130
120
110
100
90
80
70
60
50
40
30
20
10
0

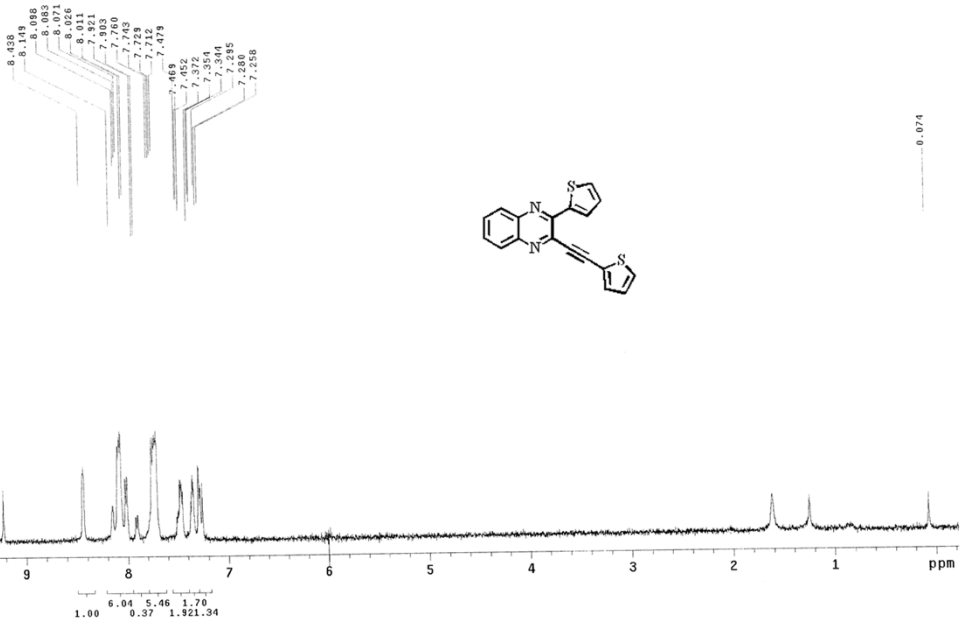
8.438
8.149
8.088
8.083
8.071
8.026
8.011
7.921
7.893
7.760
7.743
7.729
7.712
7.479
7.469
7.452
7.372
7.354
7.344
7.295
7.280
7.258
0.074
9
8
7
6
5
4
3
2
1
ppm
1.00
6.04
0.37
5.46
1.70
1.921.34

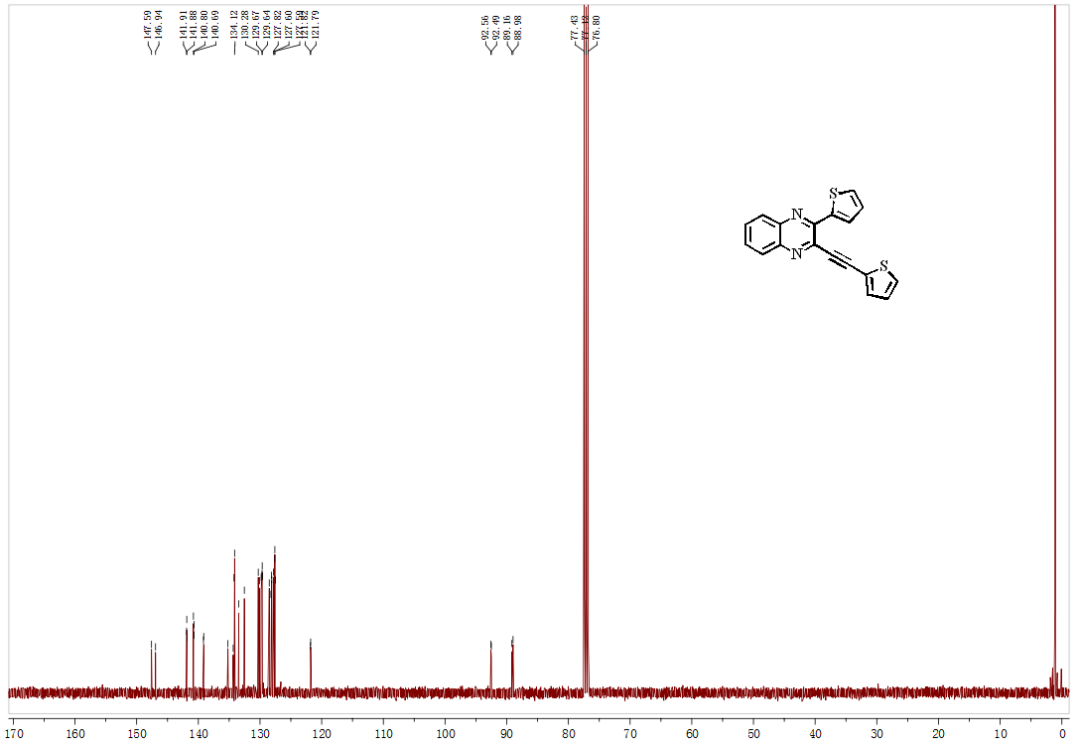

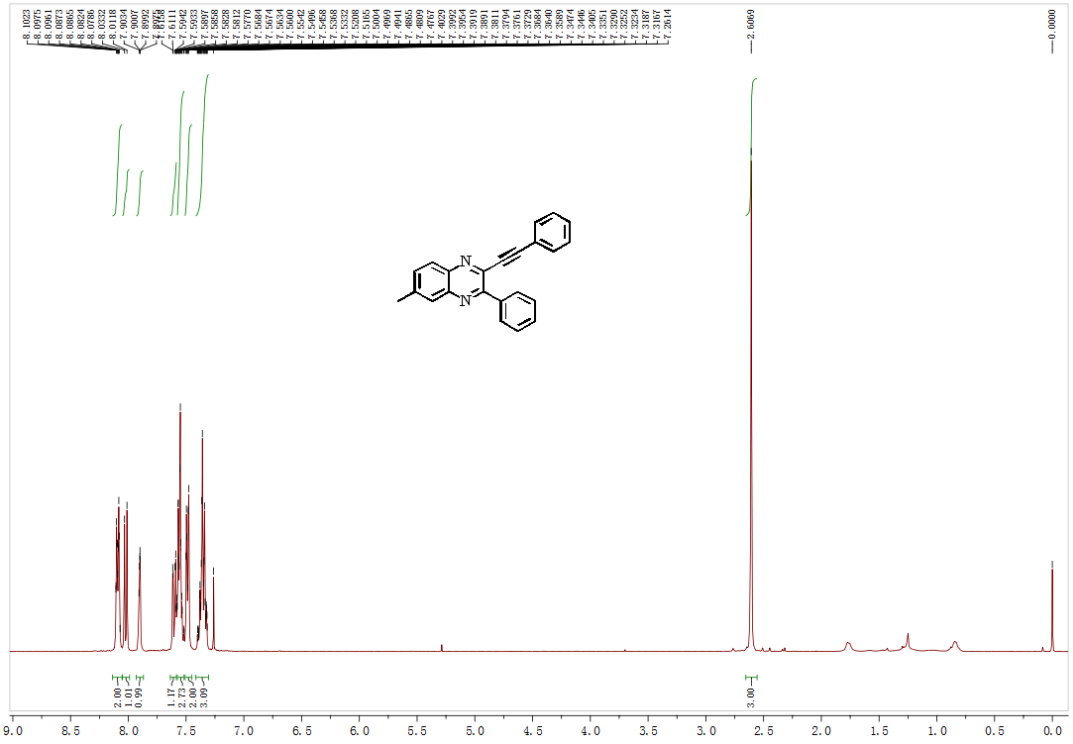

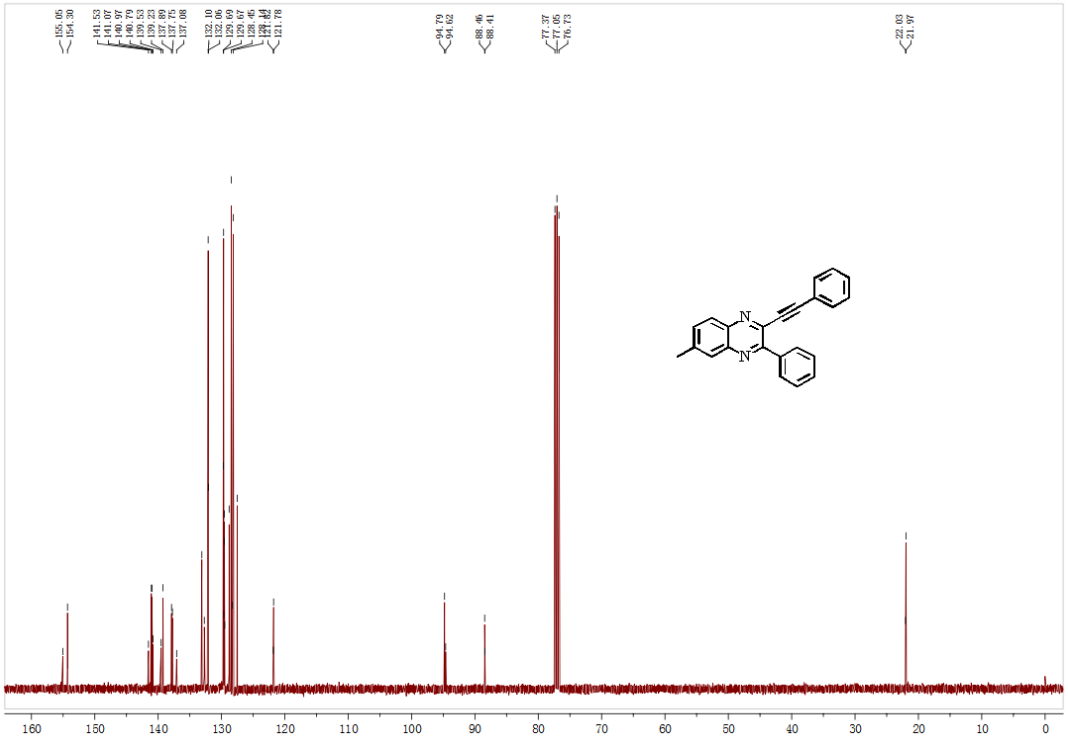

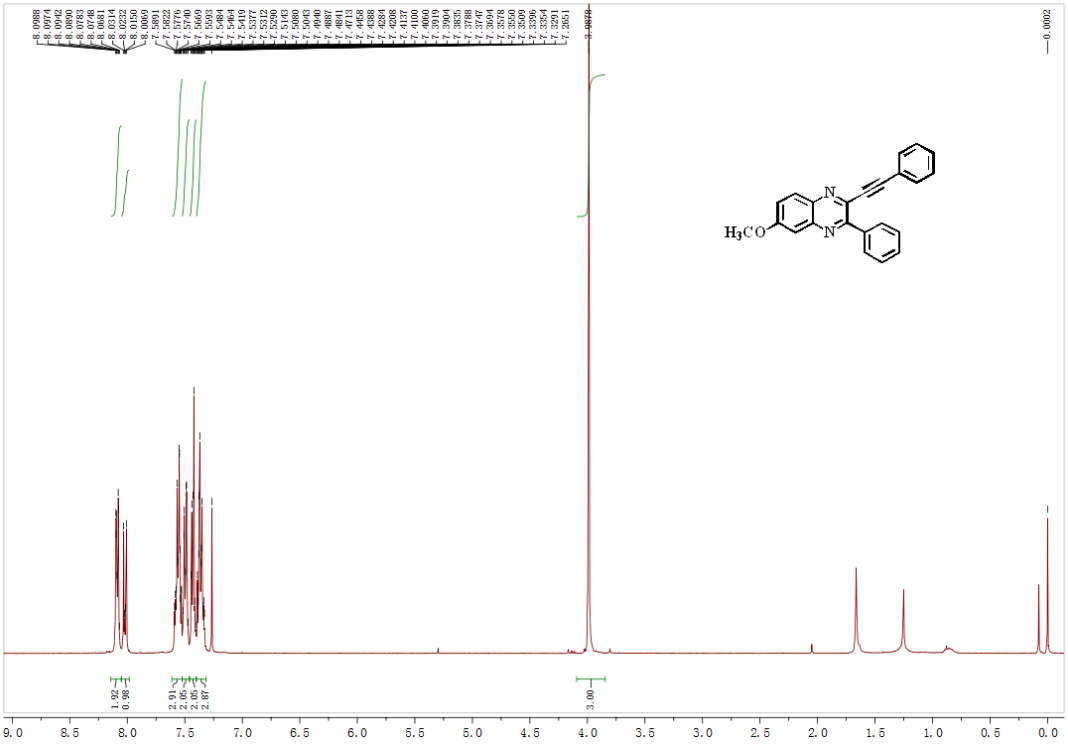

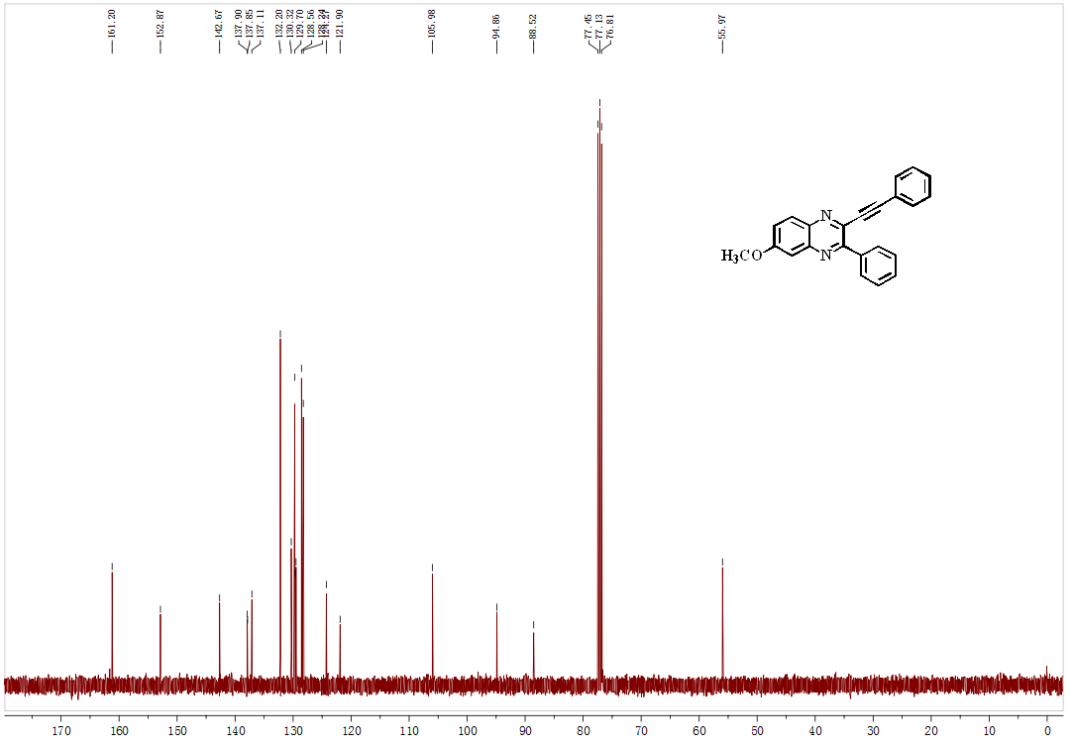
161.20
152.87
142.67
137.90
137.85
137.11
132.20
130.32
129.70
128.56
121.90
105.98
94.86
88.52
77.45
77.13
76.81
55.97
H_3CO
N
N
170
160
150
140
130
120
110
100
90
80
70
60
50
40
30
20
10
0

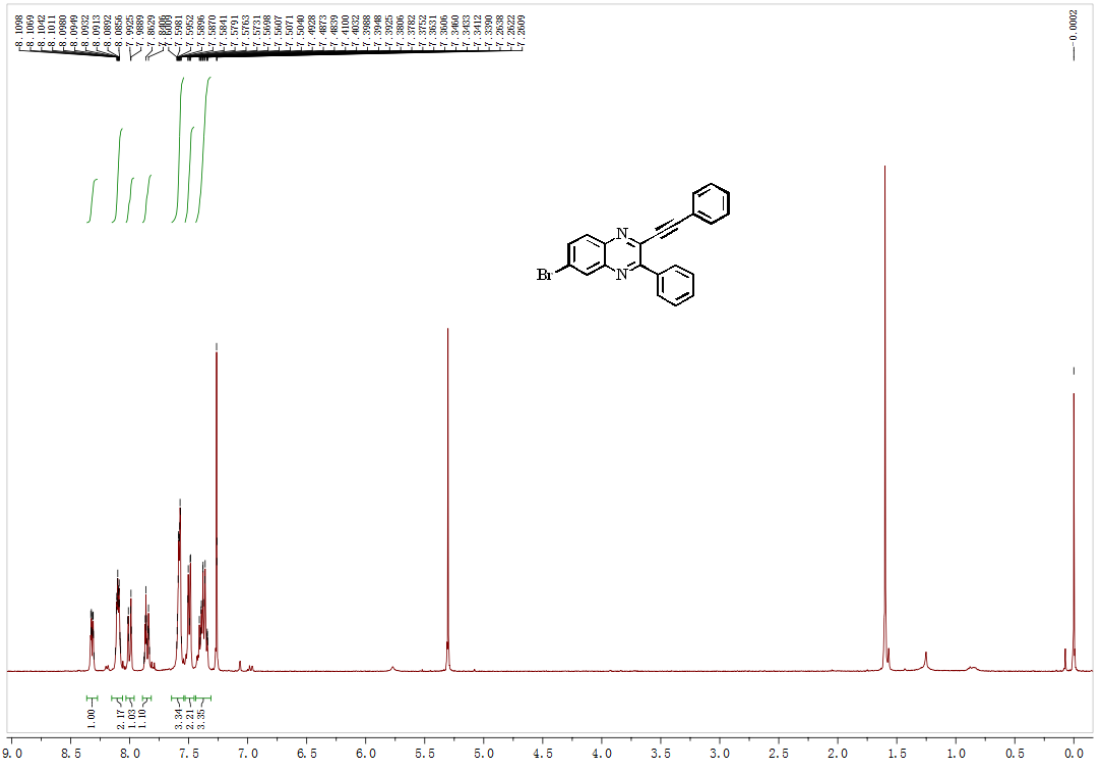
Br
N
N
1.00
2.17
1.03
1.10
3.24
3.31
3.31
9.0
8.5
8.0
7.5
7.0
6.5
6.0
5.5
5.0
4.5
4.0
3.5
3.0
2.5
2.0
1.5
1.0
0.5
0.0

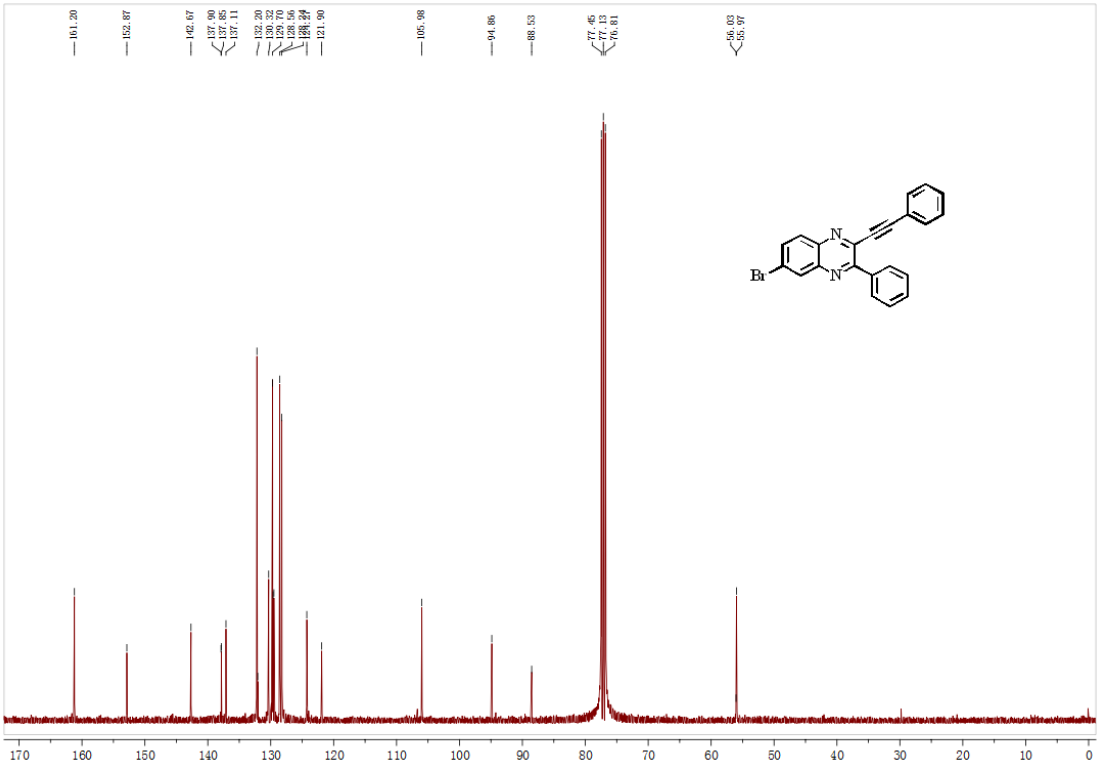

References

[1] (a) W. S. Hummers, R. E. Offeman, *J. Am. Chem. Soc.* 1958, 80, 1339; (b) D. Luo, G. Zhang, J. Liu, X. Sun, *J. Phys. Chem. C* **2011**, 115, 11327; (c) Y. Si, E. T. Samulski, *Nano Lett.* **2008**, 8, 1679; (d) R. Muszynski, B. Seger, P. V. Kamat, *J. Phys. Chem. C* 2008, 112, 5263.

[2] W. S. Hummers, R. E. Offeman, *J. Am. Chem. Soc.* **1958**, 80, 1339.

[3] (a) D. Luo, G. Zhang, J. Liu, X. Sun, *J. Phys. Chem. C* **2011**, 115, 11327 ; (b) Y. Si, E. T. Samulski, *Nano Lett.* **2008**, 8, 1679 ; (c) R. Muszynski, B. Seger, P. V. Kamat, *J. Phys. Chem. C* **2008**, 112, 5263.

[4] V. Georgakilas, A. B. Bourlinos, R. Zboril, T. A. Steriotis, P. Dallas, A. K. Stubos, C. Trapalis, *Chem. Commun.*, **2010**, 46, 1766.

[5] J. J. P. Roberts, J. A. Westgard, L. M. Cooper, R. W. Murray, *J. Am. Chem. Soc.* **2014**, 136, 10783.

[6] (a) T. Zhang, H. Zhu, J.-P. Croué, *Environ. Sci. Technol.* **2013**, 47, 2784; (b) L. Li, X. Chen, Y. Wu, D. Wang, Q. Peng, G. Zhou, Y. Li, *Angew. Chem. Int. Ed.* **2013**, 52, 11049.

[7] J. D. Perkins, J. M. Graybeal, M. A. Kastner, R. J. Birgeneau, J. P. Falck, M. Greven, *Phys. Rev. Lett.* **1993**, 71, 1621.

[8] F.A. Cotton, G. Wilkinson, Advanced Inorganic Chemistry, Interscience Publishers, London, 1974.

[9] (a) S. B. Simonsen, I. Chorkendorff, S. Dahl, M. Skoglundh, J. Sehested, S. Helveg, *J. Am. Chem. Soc.* **2010**, 132, 7968; (b) N. J. J. Johnson, A. Korinek, C. Dong, F. C. J. M. van Veggel, *J. Am. Chem. Soc.* **2012**, 134, 11068; (c) A. Simo, J. Polte, N. Pfänder, U. Vainio, F. Emmerling, K. Rademann, *J. Am.*

Chem. Soc. **2012**, 134, 18824; (d) F. Liu, J.-H. Zhu, Y.-L. Hou, S. Gao, *Chin. Phys. B* **2013**, 22, 107503; (e) C. Yang, J. Wu, Y. Hou, *Chem. Commun.,* **2011**, 47, 5130.